Tracking the Molecular Evolution of Calcium Permeability in a Nicotinic Acetylcholine Receptor

Marcela Lipovsek,*,‡,1 Angélica Fierro,†,2 Edwin G. Pérez,†,2 Juan C. Boffi,1 Neil S. Millar,3 Paul A. Fuchs,4 Eleonora Katz,1,5 and Ana Belén Elgoyhen1,6

[1]Instituto de Investigaciones en Ingeniería Genética y Biología Molecular, Dr. Héctor N Torres, Consejo Nacional de Investigaciones Científicas y Técnicas, Buenos Aires, Argentina

[2]Department of Organic Chemistry, Faculty of Chemistry, Pontificia Universidad Católica de Chile, Santiago, Chile

[3]Department of Neuroscience, Physiology and Pharmacology, University College London, London, United Kingdom

[4]Department of Otolaryngology, Head and Neck Surgery, and Center for Hearing and Balance, The Johns Hopkins University School of Medicine, Baltimore, MD

[5]Departamento de Fisiología, Biología Molecular y Celular, Facultad de Ciencias Exactas y Naturales, Universidad de Buenos Aires, Buenos Aires, Argentina

[6]Departamento de Farmacología, Facultad de Medicina, Universidad de Buenos Aires, Buenos Aires, Argentina

‡Present address: MRC Centre for Developmental Neurobiology, King's College London, London, United Kingdom

*Corresponding author: E-mail: marcela.lipovsek@gmail.com.

†These authors contributed equally to this work.

Associate editor: Yoko Satta

Abstract

Nicotinic acetylcholine receptors are a family of ligand-gated nonselective cationic channels that participate in fundamental physiological processes at both the central and the peripheral nervous system. The extent of calcium entry through ligand-gated ion channels defines their distinct functions. The $\alpha9\alpha10$ nicotinic cholinergic receptor, expressed in cochlear hair cells, is a peculiar member of the family as it shows differences in the extent of calcium permeability across species. In particular, mammalian $\alpha9\alpha10$ receptors are among the ligand-gated ion channels which exhibit the highest calcium selectivity. This acquired differential property provides the unique opportunity of studying how protein function was shaped along evolutionary history, by tracking its evolutionary record and experimentally defining the amino acid changes involved. We have applied a molecular evolution approach of ancestral sequence reconstruction, together with molecular dynamics simulations and an evolutionary-based mutagenesis strategy, in order to trace the molecular events that yielded a high calcium permeable nicotinic $\alpha9\alpha10$ mammalian receptor. Only three specific amino acid substitutions in the $\alpha9$ subunit were directly involved. These are located at the extracellular vestibule and at the exit of the channel pore and not at the transmembrane region 2 of the protein as previously thought. Moreover, we show that these three critical substitutions only increase calcium permeability in the context of the mammalian but not the avian receptor, stressing the relevance of overall protein structure on defining functional properties. These results highlight the importance of tracking evolutionarily acquired changes in protein sequence underlying fundamental functional properties of ligand-gated ion channels.

Key words: nicotinic receptors, calcium permeability, molecular evolution, hearing.

Introduction

Calcium ions extensively regulate cellular activity. To achieve this, a tight control of calcium signals in space, time, and amplitude is necessary (Laude and Simpson 2009). Ion channels that are permeable to Ca^{2+} are important players in the regulation of cellular Ca^{2+} homeostasis and in signaling intracellular Ca^{2+} effects. In contrast to voltage-gated Ca^{2+} channels, ligand-gated channels provide Ca^{2+} influx into cells at voltages close to the resting membrane potential, as is the case for nicotinic acetylcholine receptors (nAChRs) (Shen and Yakel 2009). These are members of the *Cys*-loop family of receptors, which also includes $GABA_A$, $GABA_C$, glycine, 5-hydroxytryptamine-3 (5-HT₃) and some invertebrate anionic glutamate, and histamine receptors (Dent 2006; Karlin 2002). nAChRs are expressed in the central and peripheral nervous system and are involved in pathologies, such as myasthenia, epilepsy, schizophrenia, Parkinson's disease, autism, dementia with Lewy bodies, Alzheimer's disease, and addiction (Dani and Bertrand 2007).

The nAChRs function as homo or heteropentamers. Each nicotinic subunit consists of an extracellular domain, which harbors the binding site, four transmembrane α-helices (TM1–4), and a variable intracellular region (Karlin 2002; Unwin 2005). The mechanisms and molecular determinants underlying agonist binding, channel gating, ion selectivity, and

Open Access

Article

conductance have been extensively studied (Corringer et al. 2000; Karlin 2002; Keramidas et al. 2004; Giniatullin et al. 2005; Gay and Yakel 2007; Peters et al. 2010). In particular, the determinants of calcium permeability of nAChRs have been repeatedly assigned to the TM2 region of the protein, which paves the channel pore and harbors the gate of the channel (Bertrand et al. 1993; Corringer et al. 1999; Ferrer-Montiel and Montal 1993; Fucile et al. 2000; Haghighi and Cooper 2000; Tapia et al. 2007). This mainly derives from mutagenesis studies where amino acids have been arbitrarily mutated in order to alter side chain charge (Bertrand et al. 1993; Ferrer-Montiel and Montal 1993; Corringer et al. 1999; Haghighi and Cooper 2000; Tapia et al. 2007) or hydrophobicity (Bertrand et al. 1993; Fucile et al. 2000). However, recent mutagenesis studies point toward vestibule residues as determinants of calcium permeability in Cys-loop receptors (Livesey et al. 2011; Colon-Saez and Yakel 2014). Thus, how this fundamental biological property is realized in this family of neurotransmitter receptors, at the molecular level, is still an open question.

Within the broad diversity of ligand-gated ion channels, mammalian $\alpha9\alpha10$ nAChRs are among the ones that show the highest calcium permeability (Mayer and Westbrook 1987; Kaupp and Seifert 2002; Weisstaub et al. 2002; Fucile, Sucapane, Eusebi 2006; Lipovsek et al. 2012). They play a fundamental role in controlling calcium concentration at the base of cochlear hair cells, where they serve fast synaptic transmission at the efferent-hair cell synapse, a system that controls the dynamic range of hearing (Elgoyhen and Katz 2012). The tight control of calcium entry through $\alpha9\alpha10$ nAChRs is fundamental, as the subsequent activation of calcium-dependent potassium channels hyperpolarizes hair cells to reduce cochlear amplification (Fuchs and Murrow 1992a, 1992b; Glowatzki and Fuchs 2000). Interestingly, it has recently been reported that mammalian $\alpha9\alpha10$ nAChRs have higher calcium permeability than their avian homolog (Lipovsek et al. 2012). This could relate to the different mechanisms of cochlear amplification used by mammalian versus nonmammalian species (Dallos et al. 2008). In addition, signatures of positive selection were reported for the $\alpha10$ (but not $\alpha9$) mammalian nAChR subunits using codon-based maximum-likelihood analysis (Franchini and Elgoyhen 2006). This has led to the proposal that enhanced calcium permeability of $\alpha9\alpha10$ nAChRs might be due to the evolutionarily acquired changes in the $\alpha10$ subunit (Lipovsek et al. 2012). This differential property between mammalian and chicken $\alpha9\alpha10$ nAChRs opens the unique opportunity for defining the underlying molecular determinants that shape the extent of calcium permeability of a ligand-gated ion channel, along its evolutionary history. Using ancestral sequence reconstruction, together with molecular dynamics (MD) simulations and an evolutionary-based mutagenesis strategy, we have determined that it is the $\alpha9$ (and not the $\alpha10$) subunit the one that defines the high calcium permeability of mammalian $\alpha9\alpha10$ nAChRs. Moreover, we identified three amino acid residues within the $\alpha9$ subunit that differed only in the mammalian lineage and are directly involved. Contrary to expectation, these residues are located outside the TM2

pore-lining region of the channel. Furthermore, these nonsynonymous substitutions cause an increase in calcium permeability only within the context of the mammalian, and not the avian, $\alpha9\alpha10$ receptor, stressing the relevance of overall protein structure on defining functional properties. This work unravels the molecular underpinnings of an evolutionary process with major implications for the operation of the efferent olivocochlear system. Moreover, it aids toward understanding how a fundamental property of cholinergic ligand-gated ion channels was shaped along vertebrate evolution.

Results

Calcium Permeability of the $\alpha9\alpha10$ Nicotinic Receptor Is Determined by the $\alpha9$ Subunit

The injection of Xenopus laevis oocytes with cRNAs coding for the different nAChR subunits results in the expression of functional channels on the cell membrane. The considerable size of the oocytes (~1 mm), together with the high expression level of the heterologous protein, allows measuring currents that result from channel openings in response to agonist application, using the two-electrode voltage clamp technique. With the aim of determining whether the accumulation of amino acid changes within the $\alpha10$ subunit (Franchini and Elgoyhen 2006) resulted in a preferred contribution of this subunit to the reported high calcium permeability of mammalian $\alpha9\alpha10$ nAChRs (Lipovsek et al. 2012), we first studied the relative contribution of each subunit to this property. We analyzed responses of homomeric receptors (composed only of identical subunits) heterologously expressed in Xenopus oocytes. To assess Ca^{2+} flux through recombinant nAChRs, we studied the contribution of the ICl_{Ca} to acetylcholine (Ach)-evoked responses. ICl_{Ca} is a Ca^{2+}-dependent Cl^- channel present in Xenopus oocytes, which has a high sensitivity to Ca^{2+} and is an optimal detector of calcium entry to the oocyte (Barish 1983; Miledi et al. 1989). Receptors with high Ca^{2+} permeability, such as $\alpha7$ (Seguela et al. 1993) and rat $\alpha9\alpha10$ (Elgoyhen et al. 2001) nAChRs, have a prominent contribution of ICl_{Ca} to ACh-evoked responses, compared with a modest contribution in nAChRs with lower Ca^{2+} permeability, such as $\alpha4\beta2$ and chicken $\alpha9\alpha10$ (Lipovsek et al. 2012). This can be evidenced by incubation of the oocytes with the membrane permeant fast Ca^{2+} chelator 1,2-bis(2-aminophenoxy)ethane-N,N,N′,N′-tetraacetic acid-acetoxymethyl ester (BAPTA-AM), which abolishes the Cl^- component of the total measured current. Figure 1 shows representative responses to $100\,\mu M$ ACh, at a membrane holding potential (V_{hold}) of -70 mV, before and after a 3-h incubation with BAPTA-AM. Previously reported responses of heteromeric $\alpha9\alpha10$ nAChRs (Lipovsek et al. 2012) are included for the sake of comparison (fig. 1A). ACh-evoked currents were markedly reduced in amplitude after treatment with BAPTA-AM in the case of rat $\alpha9\alpha10$ (response after BAPTA: $14.8 \pm 3.1\%$ of the initial response, $n = 12$), but remained unaltered in the case of chicken $\alpha9\alpha10$ nAChRs ($100.3 \pm 14.1\%$, $n = 6$, fig. 1A and supplementary table S1, Supplementary Material online). It has been reported that the rat $\alpha9$ homomeric receptor has high calcium permeability
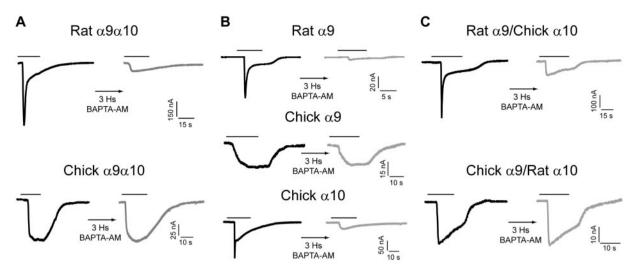
FIG. 1. Chick $\alpha 9$ containing receptors do not activate the oocyte $I\text{Cl}_{Ca}$. Representative traces of responses evoked by 100 μM ACh in oocytes expressing either heteromeric (A), homomeric (B) or hybrid (C), nAChRs, before (left—black trace) and after (right—gray trace) a 3-h incubation with the fast calcium chelator BAPTA-AM ($V_{hold} = -70$ mV; $[Ca^{2+}]_{extracellular} = 1.8$ mM). Traces are representative of $n = 4$–12 per group.

(Katz et al. 2000), similar to that of the rat $\alpha 9\alpha 10$ heteromeric receptor (Elgoyhen et al. 2001; Lipovsek et al. 2012; Weisstaub et al. 2002). Accordingly, ACh-evoked currents were markedly reduced after BAPTA-AM incubation, indicating a strong contribution of $I\text{Cl}_{Ca}$ to the initial response and therefore influx of Ca^{2+} through this homomeric receptor (fig. 1B, upper traces). Thus, the percentage of remaining response after BAPTA-AM ($14.3 \pm 2.9\%$, $n = 7$) was similar to that previously described for rat $\alpha 9\alpha 10$ nAChRs (supplementary table S1, Supplementary Material online; Elgoyhen et al. 2001; Lipovsek et al. 2012). In contrast, ACh responses remained unaffected after BAPTA-AM incubation in oocytes expressing the chicken $\alpha 9$ homomeric receptor ($99.5 \pm 15.1\%$, $n = 4$; fig. 1B, middle traces and supplementary table S1, Supplementary Material online), as observed for the chicken $\alpha 9\alpha 10$ nAChR (fig. 1A; Lipovsek et al. 2012), indicating a negligible contribution of $I\text{Cl}_{Ca}$.

Mammalian (rat and human) $\alpha 10$ subunits are not able to form functional homomeric receptors (Elgoyhen et al. 2001; Sgard et al. 2002). However, the injection of Xenopus oocytes with cRNA coding for the chicken $\alpha 10$ subunit resulted in the expression of functional receptors (fig. 1B, lower traces). ACh-evoked currents through chicken $\alpha 10$ receptors were reduced after BAPTA-AM incubation ($12.7 \pm 4.7\%$ of the initial response, $n = 10$), indicating a strong contribution of $I\text{Cl}_{Ca}$ to the ACh response and thus influx of Ca^{2+} (supplementary table S1, Supplementary Material online). These results suggest that it is the $\alpha 9$ subunit that dictates the extent of calcium permeability of the $\alpha 9\alpha 10$ nAChR. In order to examine this possibility further, we injected Xenopus oocytes with two alternative combinations of $\alpha 9$ and $\alpha 10$ subunits, so as to express interspecies hybrid receptors. ACh-evoked currents were markedly reduced after BAPTA-AM incubation, indicating a strong contribution of $I\text{Cl}_{Ca}$ to the initial response and thus influx of Ca^{2+} through the rat $\alpha 9$/chicken $\alpha 10$ hybrid receptor (fig. 1C). The percentage of response remaining after BAPTA treatment of this interspecies hybrid ($21.8 \pm 8.2\%$, $n = 5$; supplementary table S1, Supplementary Material

online) was similar to that observed with the rat $\alpha 9\alpha 10$ receptor ($P = 0.3329$; fig. 1A and supplementary table S1, Supplementary Material online). In contrast, ACh responses of the chicken $\alpha 9$/rat $\alpha 10$ hybrid receptor remained unaffected after BAPTA-AM incubation ($103.4 \pm 20.0\%$, $n = 7$; fig. 1C), similar to the behavior of the chicken $\alpha 9\alpha 10$ receptor (fig. 1A and supplementary table S1, Supplementary Material online), indicating low calcium influx.

The two-electrode voltage clamp configuration allows us to apply a voltage ramp to oocytes expressing nAChRs, measure the current through the activated channels at different holding potentials and then plot the current/voltage (I–V) curves. $\alpha 9\alpha 10$ receptors are nonspecific cation channels, permeable to Na^+, K^+ and Ca^{2+}, under physiological conditions. In order to estimate the relative Ca^{2+} permeability of recombinant receptors, we measured the reversal potential (E_{rev}) as a function of extracellular Ca^{2+} concentration (0.2–5 mM) and fitted the data to the extended Goldman–Hodgkin–Katz (GHK) equation. E_{rev} is the zero-current potential in figure 2, for example, the potential at which the current reverses sign. Only changes in extracellular concentration of permeating ions will affect the E_{rev}. For the homomeric rat $\alpha 9$ receptor, E_{rev} showed a dependence on extracellular calcium similar to that of the heteromeric rat $\alpha 9\alpha 10$ receptor (fig. 2A left panel and B; insets show a zoom near the E_{rev} for 0.5 and 5 mM Ca^{2+}). Accordingly, the fit of these data to the extended GHK equation yielded a high calcium permeability ratio (pCa/pNa, 6.1 ± 1.2, $n = 4$), like that of the rat $\alpha 9\alpha 10$ receptor (7.9 ± 0.6, $n = 11$; $P = 0.1820$; supplementary table S1, Supplementary Material online). Conversely, the pCa/pNa value for the chicken $\alpha 9$ receptor (2.6 ± 0.3, $n = 12$) was similar to that obtained for the chicken $\alpha 9\alpha 10$ receptor (2.3 ± 0.3, $n = 9$; $P = 0.5098$; fig. 2A center panel and B; supplementary table S1, Supplementary Material online) but over three times lower than that of rat $\alpha 9\alpha 10$ ($P < 0.0001$; supplementary table S1, Supplementary Material online). Finally, the chicken $\alpha 10$ homomeric receptor had a high pCa/pNa (6.9 ± 1.0, $n = 8$), similar to that of the rat $\alpha 9\alpha 10$ receptor
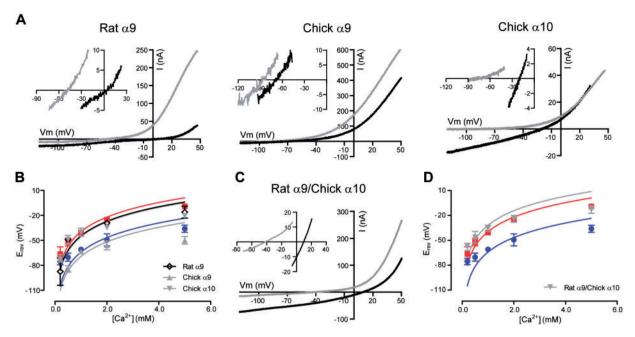
FIG. 2. Homomeric and hybrid receptors have different relative calcium permeabilities. (A) Representative I–V curves obtained by application of voltage ramps (-120 to $+50$ mV, 2 s) at the plateau of the response to 100 μM ACh in oocytes superfused with NMG$^+$-based solutions containing different Ca^{2+} concentrations (0.5 mM, gray and 5 mM, black) for oocytes expressing either rat α9 (upper left), chicken α9 (upper middle), or chicken α10 (upper right) nAChRs. Insets: Magnification near the E$_{rev}$. (B) Plot of E$_{rev}$ values as a function of extracellular Ca^{2+} concentration for rat α9, chicken α9, and chicken α10 homomeric nAChRs. E$_{rev}$ values for rat α9α10 (red) and chicken α9α10 (blue) are shown for comparison. Values are mean $\pm$ SEM of 4–12 experiments per group. Solid lines are fit to the GHK equation (see Materials and Methods). (C) Idem as in (A) for oocytes expressing rat α9/chicken α10 hybrid nAChRs. (D) Idem as in (B) for the rat α9/chicken α10 hybrid nAChR.

($P = 0.3907$; fig. 2A right panel and B; supplementary table S1, Supplementary Material online). Figure 2C shows representative I–V curves for the rat α9/chicken α10 hybrid receptor and figure 2D, E$_{rev}$ as a function of extracellular calcium concentration. Consistent with the results obtained from the evaluation of the activation of ICl_{Ca} (fig. 1C), the rat α9/chicken α10 hybrid had a high pCa/pNa (9.0 $\pm$ 1.0, $n = 7$), similar to that of the rat α9α10 receptor ($P = 0.3013$; supplementary table S1, Supplementary Material online). Thus, the chicken α10 subunit has no determinants capable of affecting the calcium permeability of the α9α10 receptor.

Figure 3 summarizes the conclusions drawn from the above experiments: Whenever a receptor has a rat α9 subunit (red circle), whether homomeric, heteromeric, or hybrid, the activation of the ICl_{Ca} is high (reduced percentage of response after BAPTA, fig. 3A) and thus the relative calcium permeability is high (fig. 3B). On the contrary, whenever a receptor contains a chicken α9 subunit (blue circle), the activation of the ICl_{Ca} is low (fig. 3A) and thus the relative calcium permeability is low (fig. 3B). Therefore, the high relative calcium permeability of the mammalian α9α10 nicotinic receptor results from molecular determinants present in the α9 subunit and not the α10 subunit as previously suggested by the codon-based maximum-likelihood analysis of positive selection (Franchini and Elgoyhen 2006; Lipovsek et al. 2012).

Molecular Evolution of Mammalian α9 Subunits

The experiments described in the first section allocate the differences in the extent of calcium permeability of α9α10

receptors to the α9 subunit. However, previous analysis performed on α9 coding sequences from 13 vertebrate species found no evidences of positive selection in any region of the α9 protein or in any lineage of the vertebrate phylogeny (Franchini and Elgoyhen 2006). We now extend this analysis to α9 subunit coding sequences from 52 vertebrate species, including the relevant addition of six avian/reptile species. The alignment in supplementary figure S1, Supplementary Material online, shows all extant sequences used in the analysis; accession numbers are listed in supplementary table S2, Supplementary Material online. We performed the branch-site test of positive selection, which detects the presence of sites under positive selection within a given gene in specific lineages of a phylogeny (Yang and Nielsen 2002; Zhang et al. 2005). The mammalian, eutherian, and sauropsid lineages were used as foreground branches in separate analyses. As shown in table 1, we found no statistically significant evidence of positive selection on the α9 subunit coding sequence. Nonetheless, as the functional studies unequivocally indicate that differences in calcium permeability are determined by the α9 subunit, these could be conferred by the small number of amino acid differences observed between lineages and that are not detected by the positive selection analyses.

In order to further our insight into the evolutionary history of the α9 subunit coding sequences and their limited number of nonsynonymous substitutions across lineages, we performed an ancestral sequence reconstruction for all the nodes of the phylogeny depicted in supplementary figure S2, Supplementary Material online. Our aim was to pinpoint the occurrence of amino acid substitutions specific to each
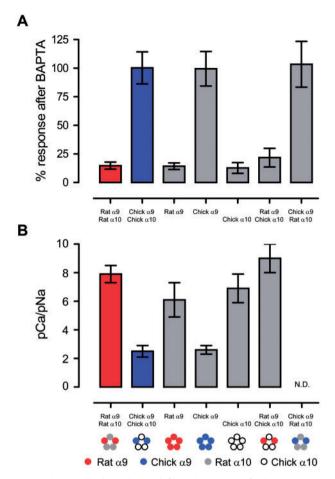
Fig. 3. The $\alpha 9$ nAChR subunit defines the extent of calcium permeability of $\alpha 9 \alpha 10$ receptors. (A) Percentage response to $100\,\mu M$ ACh after 3-h incubation with the fast calcium chelator BAPTA-AM for heteromeric, homomeric, and hybrid nAChRs. The percentage of the initial response remaining after BAPTA incubation was determined for each oocyte individually and then averaged for each receptor. Values are mean $\pm$ SEM. (B) Relative calcium permeability (pCa/pNa) as determined from fitting E_{rev} data, as a function of extracellular calcium concentration, to the GHK equation extended to include divalent cations. Values are mean $\pm$ SEM. Note that whenever a rat $\alpha 9$ subunit is present calcium permeability is high and whenever a chicken $\alpha 9$ subunit is present the calcium permeability is low.

Table 1. Likelihood Value Estimates for the Branch-Site and Null Hypothesis Models.

Branch Site Models	Log Likelihood	LRT	$P(\chi^2_1)$
Mammalia			
Branch site	−20,543.177331	0.008944	0.9246
Null hypothesis	−20,543.186275		
Eutheria			
Branch site	−20,546.529218	0.112204	0.7376
Null hypothesis	−20,546.641422		
Sauropsida			
Branch site	−20,548.677492	0	1
Null hypothesis	−20,548.677494		

NOTE.—The branch-site test for positive evolution was conducted separately three times using mammals (Mammalia), placental mammals (Eutheria), and birds/reptiles (Sauropsida) as the foreground lineage. LRT = $2 \times (\ln LH_A - \ln LH_0)$. H_A, branch-site model; H_0, null hypothesis; ln L, log-likelihood.

major group. The alignment of supplementary figure S1, Supplementary Material online, shows all extant sequences used in the analysis, together with the predicted ancestral sequences of the major nodes.

Overall, a greater degree of divergence from the common amniote ancestor was observed for the mammalian than for the sauropsid (birds and reptiles) lineage (see also branch lengths in supplementary fig. S2, Supplementary Material online). A close inspection of the alignment of extant sequences and those predicted for the major nodes showed that, when comparing mammalian versus sauropsid $\alpha 9$ amino acid sequences, both branching from the ancestral amniote, 42 sites showed nonsynonymous branch-specific substitutions (highlighted in the alignment). Supplementary table S3, Supplementary Material online, shows the character state and its corresponding marginal posterior probability for each of these sites for all the major nodes of the phylogeny and representative species of each group. Figure 4A summarizes the evolutionary history of these sites, showing only residues corresponding to the extant rat and chicken $\alpha 9$ sequences, the predicted ancestral sequences for their corresponding groups (Eutheria and Diapsida, respectively), and the predicted common amniote $\alpha 9$ ancestral sequence. The amniote ancestral sequence shared 36 of these 42 amino acids with the diapsid (and sauropsid) lineage. On the other hand, it only shared six amino acids with eutheria (five with Boreoeutheria) (fig. 4A). The observed asymmetry of sequence divergence after the split from the ancestral amniote suggests that the high calcium permeability observed on mammalian $\alpha 9 \alpha 10$ receptors might be the divergent character state; that is, the $\alpha 9 \alpha 10$ receptor of the ancestral amniote may have had low calcium permeability. If this were the case, some of the nonsynonymous substitutions that accumulated along the evolutionary history of the mammalian lineage should have bestowed the high calcium permeability observed in $\alpha 9 \alpha 10$ receptors of extant mammals.

Three Mammalian-Specific Amino Acid Substitutions Confer High Calcium Permeability to Mammalian $\alpha 9 \alpha 10$ nAChRs

In order to determine which of the 37 nonsynonymous substitutions acquired during the evolutionary history of mammalian $\alpha 9$ subunits are responsible for the resultant increase in calcium permeability, we first singled out those differing residues located in regions of the receptor known to affect ion selectivity (highlighted in blue in fig. 4B). Two residues are located in the extracellular vestibule (D110 and S127), four at or flanking the TM2 pore-lining domain (A264(-4′), I275(7′), M279(11′), and A292(24′)), whereas the remaining seven residues (K433, L435, K436, T441, N442, S443, and S446) are in the membrane associated (MA) α-helix of the intracellular domain (rat $\alpha 9$ numbering—and for the TM2 domain, numbering after Miller [1989]). The phylogeny of figure 4C shows the evolutionary history of the six sites located at the extracellular and TM2 domains, clearly illustrating that the nonsynonymous substitutions are exclusive to the mammalian lineage.
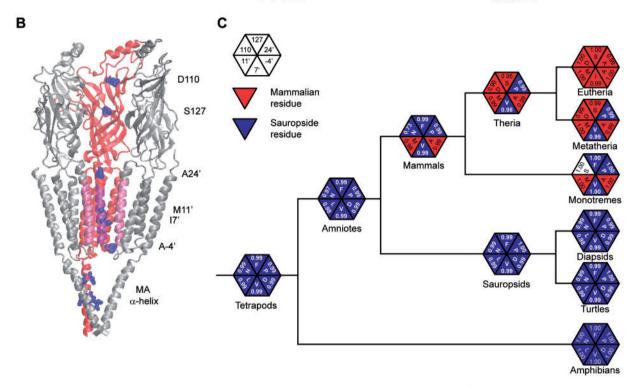
Fig. 4. Ancestral sequence reconstruction allocates nonsynonymous substitutions to the mammalian lineage. (A) Amino acid residues present at the 42 clade-specific sites for the rat and chicken α9 extant sequences and eutheria, diapsida, and amniote predicted ancestral α9 sequences. Red, mammalian residue; blue, sauropsid residue; green, tetrapod residue. Note that the majority of the residues present in the predicted ancestral amniote sequence corresponds to sauropsid residues. (B) Structure of the *Torpedo californica* nAChR (2bg9; Unwin 2005) showing, in blue, the homologous location of the sites that present clade-specific nonsynonymous substitutions and are positioned along the ion conduction pathway. Clade-specific sites K433, L435, K436, T441, N442, S443, and S446 of the MA α-helix are also highlighted in blue. Two subunits were removed for a better view of the channel. The pore-lining transmembrane domain 2 α-helices are highlighted in pink. (C) Schematic phylogeny depicting the evolutionary history of the six sites analyzed by site-directed mutagenesis: 110 and 127 at the extracellular vestibule, and 24′, 11′, 7′, and −4′ at, or flanking the TM2 domain (rat α9 and Miller 1989 numbering). For each site, the character state (amino acid) and the posterior probability of the marginal reconstruction are shown. Red, mammalian residue; blue, sauropsid residue; white, residue present only in monotremes.

To test the effect on calcium permeability of the mammalian branch-specific nonsynonymous substitutions located in the extracellular and transmembrane domains, each amino acid present on the rat α9 subunit was reversed to the corresponding residue on the predicted ancestral amniote subunit. To evaluate the effect of all the substitutions encountered in the highly variable intracellular domain, including the seven clade-specific substitutions located in the more conserved MA α-helix, we constructed a chimeric subunit in which the entire intracellular domain of the rat α9 subunit was replaced by the intracellular domain of the chicken α9 subunit. Mutant or chimeric rat α9 subunits were coinjected with the wild-type rat α10 subunit. Calcium permeability was evaluated, as before, by analyzing the activation of the oocyte's ICl_{Ca} (fig. 5A and supplementary table S1, Supplementary Material online) and by determining the relative calcium permeability (pCa/pNa; fig. 5B and supplementary fig. S3, Supplementary Material online).

The rat α9α10 mutant receptor bearing the D110N substitution, located at the extracellular vestibule, activated the oocyte's ICl_{Ca} to a lesser extent (59.8 ± 11.9% of remaining current after BAPTA treatment, $n = 6$; fig. 5A left panel and supplementary table S1, Supplementary Material online) than did the rat α9α10 wild-type counterpart (14.8 ± 3.1%, $n = 12$, $P = 0.0002$; fig. 1A and supplementary table S1, Supplementary Material online), indicating a reduction in calcium influx. This substitution also reduced the relative calcium permeability of the mutant receptor (5.5 ± 0.3, $n = 7$; fig. 5B left panel and supplementary table S1, Supplementary Material online), when compared with the wild-type rat
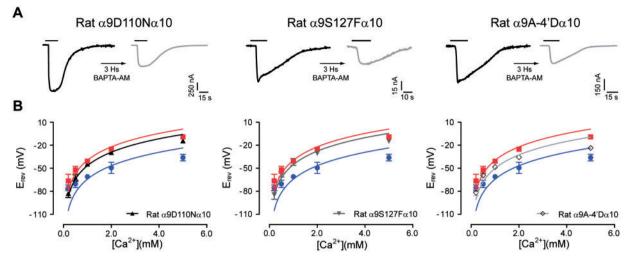
Fig. 5. Mutations in the extracellular vestibule and the exit of the channel pore alter calcium permeability of the rat $\alpha9\alpha10$ receptor. (A) Representative traces of responses evoked by 100 μM ACh in oocytes expressing rat $\alpha9\alpha10$ single mutant receptors: rat $\alpha9$D110N$\alpha10$ (left panel), rat $\alpha9$S127F$\alpha10$ (middle panel), and rat $\alpha9$ A-4'D$\alpha10$ (right panel), before (left—black trace) and after (right—gray trace) a 3-h incubation with the fast calcium chelator BAPTA-AM ($V_{hold}=-70$ mV; $[Ca^{2+}]_{extracellular}=1.8$ mM). Traces are representative of $n=4$–6 per group. (B) Plot of E_{rev} values as a function of extracellular Ca^{2+} concentration for rat $\alpha9$D110N$\alpha10$ (left panel), rat $\alpha9$S127F$\alpha10$ (middle panel), and rat $\alpha9$ A-4'D$\alpha10$ (right panel) single mutant receptors. E_{rev} values for rat $\alpha9\alpha10$ (red) and chicken $\alpha9\alpha10$ (blue) are shown for comparison. Values are mean $\pm$ SEM of 5–11 experiments per group. Solid lines are fit to the GHK equation (see Materials and Methods).

$\alpha9\alpha10$ receptor (7.9 $\pm$ 0.6, $n=11$, $P=0.0206$). The S127F substitution also produced a significant reduction of calcium influx (49.4 $\pm$ 8.4% of remaining current after BAPTA, $n=5$, $P=0.0002$; fig. 5A middle and supplementary table S1, Supplementary Material online) and a significant decrease in pCa/pNa (5.4 $\pm$ 0.4, $n=5$, $P=0.0408$; fig. 5B middle and supplementary able S1, Supplementary Material online), when compared with the wild-type rat $\alpha9\alpha10$ receptor. These results indicate that these two residues located in the vestibule of the receptor, away from the channel pore, contribute to the selectivity for divalent versus monovalent cations in the rat $\alpha9\alpha10$ receptor.

To further analyze whether these vestibule residues in fact interact with passing calcium ions, we performed an MD simulation on a homology model of the rat $\alpha9\alpha10$ receptor. We applied a force vector to a hydrated calcium ion and measured such force as the calcium was pushed into the vestibule. The increase in force amplitude needed for the calcium to move deeper into the channel, as simulation time progresses, is an indicator of the strength of its interaction with vestibule residues. Figure 6A shows a plot of the force associated with calcium passage through the channel as a function of simulation time (1.25 ns—five replicates). The peaks (red arrows at 0.1, 0.7, and 1.1 ns) indicate simulation times where calcium interacts more strongly with particular residues within the vestibule. Thus, as it transverses the extracellular vestibule, a calcium ion interacts first with residues D110 and E129 of the $\alpha9$ subunit (fig. 6B, at 0.1 ns) and residues F39 and Y42 of the $\alpha10$ subunit (all numbering after rat $\alpha9$). Then, it interacts with residues D124/D125 of the $\alpha9$ subunit (fig. 6C, at 0.7 ns). Finally, the calcium ion interacts with a number of highly conserved residues located at the mouth of the channel pore: Residues E294 of the $\alpha9$ and $\alpha10$

subunits, located in the respective TM2–TM3 loops, and residues N74 of the $\alpha9$ subunit and D71 and N74 of the $\alpha10$ subunit, located in the respective $\beta1$–$\beta2$ loops (fig. 6D, at 1.1 ns). Thus, this evidence shows a direct interaction of residue D110 with permeating calcium. In addition, it positions residue S127 between two consecutive interaction sites, E129 and D124/D125, denoting the relevance of the two mammalian specific substitutions, located at the receptor vestibule, on the calcium permeation mechanism.

When considering the residues located at or near the TM2 pore-lining domain of the rat $\alpha9\alpha10$ receptor, neither substitutions A24'P, I7'V nor M11'L had a significant effect on either the activation of the oocyte's ICl_{Ca} or the relative calcium permeability (pCa/pNa) (supplementary table S1, Supplementary Material online, and fig. S3). In contrast, the A-4'D substitution, located in an intracellular ring of charged residues (Imoto et al. 1988), produced a significant decrease in the activation of the oocyte's ICl_{Ca} (59.5 $\pm$ 5.9% of current remaining after BAPTA treatment, $n=4$; fig. 5A right and supplementary table S1, Supplementary Material online), when compared with the rat $\alpha9\alpha10$ wild-type counterpart (14.8 $\pm$ 3.1%, $n=12$, $P<0.0001$; fig. 1A and supplementary table S1, Supplementary Material online). Accordingly, the A-4'D substitution also produced a significant reduction of the relative calcium permeability (4.8 $\pm$ 0.3, $n=11$; fig. 5B right panel and supplementary table S1, Supplementary Material online), when compared with the rat $\alpha9\alpha10$ wild-type receptor (7.9 $\pm$ 0.6, $n=11$, $P=0.0002$). Finally, the complete exchange of the intracellular domain, encompassing the seven clade-specific substitutions of the MA α-helix to render the rat $\alpha9$(IC-chicken $\alpha9$)$\alpha10$ chimeric receptor, had no effect on relative calcium permeability (supplementary table S1, Supplementary Material online, and fig. S3).
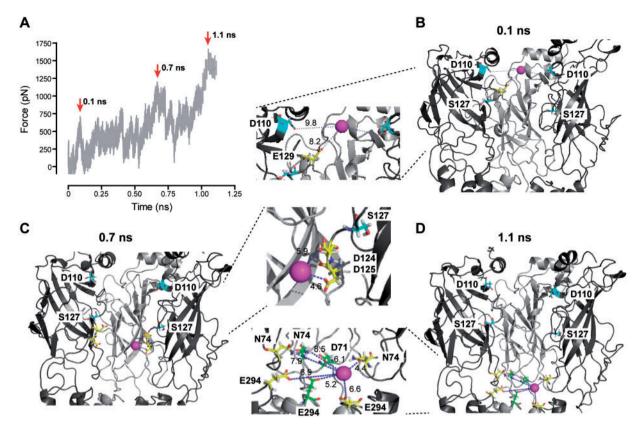
Fig. 6. MD simulation shows calcium interaction with residues in the extracellular vestibule. (A) Force associated with hydrated calcium passage through the channel vestibule, as a function of simulation time. Red arrows indicate force peaks that denote interactions with channel residues at different times along the trajectory. (B–D) Structure of the homology model of the rat $\alpha 9\alpha 10$ receptor showing the passage of a calcium ion (purple) through the channel vestibule at different simulation times. Residues D110 and S127, analyzed by site-directed mutagenesis, are highlighted in light blue. Other residues interacting with the calcium ion are highlighted in yellow ($\alpha 9$ subunit) and green ($\alpha 10$ subunit). Dark gray, $\alpha 9$ subunits; light gray, $\alpha 10$ subunit. Two $\alpha 10$ subunits and water molecules were removed for a better view of the vestibule. A close-up of the interactions is shown in the middle panels. Dotted blue lines indicate interactions of the calcium ion with channel residues; the corresponding interaction distances are shown alongside in Å. (B) 0.1 ns: calcium interacts with residues D110 and E129 of the $\alpha 9$ subunit and with residues F38 and Y41 of one of the removed $\alpha 10$ subunits. (C) 0.7 ns: calcium interacts with D124 and D125 of the $\alpha 9$ subunit. (D) 1.1 ns: calcium interacts with residues E294 of the $\alpha 9$ subunit and E293 of the $\alpha 10$ subunit, located in the respective TM2–TM3 loops, and with residues N74 of the $\alpha 9$ subunit and D70 and N73 of the $\alpha 10$ subunit, located in the respective $\beta 1$–$\beta 2$ loops.

In summary, only substitutions D110N, S127F, and A-4′D reduced the calcium permeability of the rat $\alpha 9 10$ wild-type receptor, albeit none to the full extent of the low calcium permeability observed for the chicken $\alpha 9\alpha 10$ nAChR. Therefore, we subsequently incorporated all three substitutions into the rat $\alpha 9$ subunit. This triple mutant rat $\alpha 9\alpha 10$ receptor showed low calcium influx ($100.5 \pm 13.9\%$ of remaining current after BAPTA, $n = 6$; fig. 7A and supplementary table S1, Supplementary Material online), similar to that observed for the chicken $\alpha 9\alpha 10$ nAChR ($P = 0.9924$). Accordingly, the presence of all three substitutions reduced almost 3-fold the relative calcium permeability of the rat $\alpha 9\alpha 10$ triple mutant nAChR to a pCa/pNa value (3.2 ± 0.4, $n = 7$) comparable to that of the chicken counterpart (2.3 ± 0.3, $n = 9$, $P = 0.0541$; fig. 7B and supplementary table S1, Supplementary Material online). Altogether, these results show that the occurrence of only three nonsynonymous substitutions within the $\alpha 9$ subunit was sufficient to increase the calcium permeability of the mammalian $\alpha 9\alpha 10$ receptor, an

evolutionary event that occurred after the split from the amniote ancestor.

The Increase in Calcium Permeability Is Exclusive to the Mammalian Lineage

The three amino acids identified as determinants of the increase in calcium permeability of mammalian $\alpha 9\alpha 10$ receptors represent nonsynonymous substitutions, which are exclusive to the mammalian lineage. We next asked whether the introduction of these amino acids into the chicken $\alpha 9$ subunit can lead to a high calcium permeable chicken $\alpha 9\alpha 10$ receptor. Accordingly, we mutated each one of the three amino acid residues in the chicken $\alpha 9$ subunit to the corresponding residue present in mammalian $\alpha 9$ subunits and expressed mutant receptors with the wild-type chicken $\alpha 10$ subunit.

Substitutions N110D and F127S in the extracellular vestibule did not modify the relative calcium permeability, when mutated individually (fig. 8A and supplementary table S1,
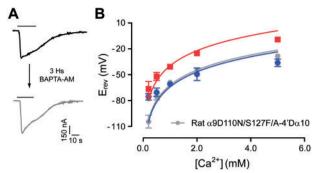
Fig. 7. The rat α9N110D/S127F/A-4'Dα10 triple mutant shows avian-like low calcium permeability. (A) Representative traces of responses evoked by 100 μM ACh in oocytes expressing the rat α9N110D/S127F/A-4'Dα10 triple mutant receptor, before (left—black trace) and after (right—gray trace) a 3-h incubation with the fast calcium chelator BAPTA-AM ($V_{hold} = -70$ mV; $[Ca^{2+}]_{extracellular} = 1.8$ mM). Traces are representative of $n = 6$. (B) Plot of E_{rev} values as a function of extracellular Ca^{2+} concentration for the rat α9N110D/S127F/A-4'Dα10 triple mutant receptor. E_{rev} values for rat α9α10 (red) and chicken α9α10 (blue) are shown for comparison. Values are mean $\pm$ SEM of 7–11 experiments per group. Solid lines are fit to the GHK equation (see Materials and Methods).

Supplementary Material online). The D-4'A substitution produced a significant increase in the relative calcium permeability (pCa/pNa: 3.7 ± 0.4, $n = 11$; fig. 8B and supplementary table S1, Supplementary Material online), when compared with the wild-type chicken α9α10 receptor (2.3 ± 0.3, $n = 9$, $P = 0.0070$). When N110D and F127S were incorporated together with the D-4'A substitution, the relative calcium to monovalent permeability did not differ from that of the chicken wild-type receptor (pCa/pNa $= 2.7 \pm 0.3$, $n = 6$; $P = 0.3238$; fig. 8B). These results indicate that the introduction of the mammalian-specific substitutions within the context of the chicken α9α10 receptor does not reproduce the high calcium permeability described for mammalian α9α10 receptors, and further support the conclusion that the increased calcium permeability of α9α10 nAChRs is a mammalian-specific event.

In order to further explore a plausible underlying mechanism for this paradoxical observation, we generated homology models for rat and chicken α9α10 wild-type and mutated receptors at positions 110, 127, and 4' and performed an analysis of the electrostatic potential of channel vestibules. Figure 9A shows the rat α9α10 wild-type receptor as an example; shaded in gray is the electrostatic potential of a longitudinal plane that cuts midsagitally through the receptor (the position of the plane is shown in the rotated upper view of the receptor in the left panel). The values for the potential were measured along a central Z axis (dotted line in fig. 9A) and are plotted, for all four receptors, in figure 9B. At close proximity to the mutations (purple asterisks) we observed only slight modifications of the electrostatic potential, albeit of the expected sign; for example, the change of the negative D110 and polar S127 of the rat α9 subunit, for the polar N and hydrophobic F, resulted in a less negative potential, whereas the opposite changes within the chicken α9 subunit caused

the reverse effect. Noticeably, these mutations had a stronger long range effect on the electrostatic potential at the deepest portion of the vestibule, immediately before the entrance to the transmembrane region (TM), the region that corresponds to the third calcium interaction site, at 1.1 ns of simulation time, as described in the MD simulations (see fig. 6). Thus, in the case of the rat α9α10 receptor, the presence of the D110N and S127F substitutions decreased the electrostatic potential in this deep region of the vestibule, to an extent similar to that of the chicken wild-type α9α10 receptor in accordance with the predicted, and observed, reduction in calcium permeability. On the contrary, the reverse substitutions, N110D and F127S, on the chicken α9α10 receptor did not bring the electrostatic potential closer to the less electronegative potential observed for the rat wild-type receptor, but further apart, in accordance with the lack of increase in calcium permeability seen for the mutant chicken α9α10 receptor. This further supports the conclusion that the accumulation of nonsynonymous substitutions within the α9 subunit which affect calcium permeability is a mammalian-specific event.

Discussion

This work unravels, at the molecular level, the evolutionary history that led to the acquisition of high calcium permeability of mammalian α9α10 nAChRs. As determined by ancestral sequence reconstruction, and functional and structural analyses, three mammalian-specific nonsynonymous substitutions present at the extracellular vestibule and at the exit of the channel pore of the α9 subunit are directly involved. Moreover, we show that these three critical substitutions only increase calcium permeability in the context of the mammalian (rat), and not avian (chicken), receptor. This highlights the importance of overall protein structure on defining functional properties. It is worth noting that the codon-based maximum-likelihood analysis failed to detect signatures of positive selection on the α9 subunits. Given the functional relevance of the extent of calcium permeability of α9α10 receptors for the operation of the efferent olivocochlear system (Elgoyhen and Katz 2012; Lipovsek et al. 2012, and discussed below) and the experimental evidence presented here that identifies nonsynonymous substitutions specific for the mammalian α9 subunits as directly involved in this property, we suggest that this is a case of plausible phenotypic adaptation in the absence of sequence-based signals (Hughes 2008). This has been reported before for vertebrate opsins (Yokoyama et al. 2008) and voltage sensitive phosphatases (Sutton et al. 2012). Moreover, our results open numerous questions as to what, if any, were the functional consequences of the strong signals of positive selection reported for the α10 subunits (Franchini and Elgoyhen 2006; Lipovsek et al. 2012).

Molecular Evolution of Calcium Permeability of α9α10 Receptors

Historically, the study of structure–function properties of neurotransmitter receptors, though based on structural models, has taken a "trial and error" approach, in which the participation of a residue was arbitrarily tested by
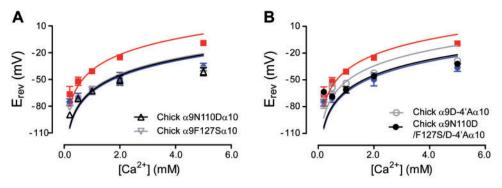
Fig. 8. Mammalian-specific mutations do not increase the calcium permeability of the chicken $\alpha9\alpha10$ receptor. Plot of E_{rev} values as a function of extracellular Ca^{2+} concentration for chicken $\alpha9N110D\alpha10$ and chicken $\alpha9F12SF\alpha10$ extracellular vestibule mutants (A) and chick $\alpha9D-4'A\alpha10$ TM1–TM2 loop mutant and chicken $\alpha9D110N/F127S/D-4'A\alpha10$ triple mutant receptor (B). E_{rev} values for rat $\alpha9\alpha10$ (red) and chicken $\alpha9\alpha10$ (blue) are shown for comparison. Values are mean $\pm$ SEM of 5–11 experiments per group. Solid lines are fit to the GHK equation (see Materials and Methods).
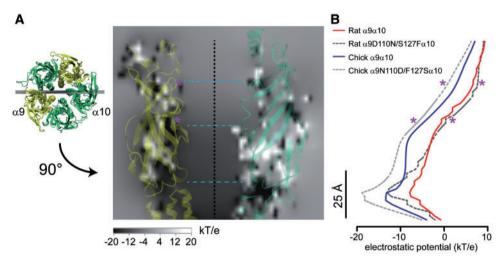

Fig. 9. Homology modelling shows that point amino acid substitutions in the extracellular domain have long range effects on the electrostatic potential. (A) Homology model of the rat $\alpha9\alpha10$ wild-type receptor showing, in a gray scale, the electrostatic potential at a longitudinal plane midsagital to the vestibule. Location of the plane is shown on an upper view of the receptor (left panel). Only the subunits at the plane of the section are shown. The dotted black line denotes the location of the central Z axis. The dotted light blue lines denote the location of the three sites of calcium interaction corresponding to 0.1 -, 0.7 - and 1.1-ns simulation times, as depicted in figure 6. Position of the two amino acid substitutions studied is denoted by purple asterisks. (B) Electrostatic potential determined at the central Z axis for rat and chicken $\alpha9\alpha10$ wild-type and mutant receptors, spanning the entire length of the vestibule. Purple asterisks denote the location of substituted residues 110 and 127.

site-directed mutagenesis. Even though this approach has been successful in describing many properties of nAChRs (Corringer et al. 2000), such mutations are not necessarily related to the evolutionary processes that shaped the primary structure, and hence, the functional characteristics of the different subunits. Thus, the phylogenetic difference in calcium permeability between rat and chicken $\alpha9\alpha10$ nAChRs, together with the ancestral sequence reconstruction, provides a unique roadmap to study how evolutionary processes have shaped this functional property.

Following the initial notion that the TM2 α-helices line the channel pore (Leonard et al. 1988) and that the TM2 flanking rings of charged residues, at positions -4', -1', and 20', are crucial determinants of channel conductance (Imoto et al. 1988), the molecular determinants of ion permeation of *Cys*-

loop receptors were, almost axiomatically, searched for and allocated to the pore-lining TM2 α-helices and flanking rings (Imoto et al. 1991; Villarroel et al. 1991; X Konno et al. 1991; Cohen et al. 1992; Galzi et al. 1992; Villarroel and Sakmann 1992; Wang and Imoto 1992; Bertrand et al. 1993; Jensen et al. 2005). For calcium permeability in particular, the participation of residues at sites 7', 9', 12', 16', 17' of the TM2 domain, -1' at the intermediate ring, and 20' at the extracellular ring has been reported for $\alpha7$, $\alpha4\beta2$, $\alpha3\beta4$ and/or $\alpha1\beta1\delta\epsilon$ nAChRs (Galzi et al. 1992; Bertrand et al. 1993; Fucile et al. 2000; Haghighi and Cooper 2000; Fucile, Sucapane, Grassi, et al. 2006; Di Castro et al. 2007; Tapia et al. 2007). Our sequence analysis shows that the TM2 domain and flanking regions are highly conserved in $\alpha9\alpha10$ nAChRs (see Lipovsek et al. 2012 for $\alpha10$ alignments and supplementary fig. S1, Supplementary

Material online, for α9 alignments), with the exception of sites -4′, 7′, 11′, and 24′ of the α9 subunit, studied in this work. The observation that mutation of residues located at positions 7′, 11′, and 24′ to their amniote ancestral state does not alter calcium permeability indicates that the TM2 region was not affected by the evolutionary process that rendered a high calcium permeable mammalian α9α10 nAChR.

The finding that residue A-4′, of the intracellular ring at the exit of the channel pore, is a determinant of calcium permeability of α9α10 nAChRs also differs from that reported for other nicotinic receptors (Corringer et al. 1999; Haghighi and Cooper 2000). It is important to note that this site is highly conserved among nAChRs and that α9 subunits are unique in showing a branch-specific substitution at this position, with mammalian α9 subunits being the only ones bearing a nonpolar uncharged residue (alanine). The increase in calcium permeability, due to the A for D nonsynonymous substitution in mammalian α9 subunits, probably results from a reduced negative electrostatic potential at the end of the pore region of the channel that would otherwise interfere with the exit of calcium. However, this effect is highly dependent upon the overall protein context, as the same D for A substitution does not affect the extent of calcium permeability of the α3β4 receptor (Haghighi and Cooper 2000) or of the highly calcium permeable α7 receptor (Corringer et al. 1999).

The participation of the extracellular vestibule of nAChRs in ion conductance and selectivity was proposed early on by theoretical modeling (Dani 1986). MD simulations, performed on a homology model of the muscle nAChR, revealed the interaction of three rings of residues located within the extracellular vestibule (positions E83, D97, and N47 of the human α1 subunit) with passing sodium ions (Wang et al. 2008). Moreover, the innermost ring has been implicated in calcium permeability in the human 5-HT$_{3A}$ high conductance mutant receptor and the rat α7 nAChR (Hansen et al. 2008; Livesey et al. 2011; Colon-Saez and Yakel 2014). The present MD simulations, performed on a homology model of the rat α9α10 nAChR, additionally show a close interaction of a permeating calcium ion with residues located at three sites homologous to those three rings of residues. Moreover, we provide experimental evidence showing that two residues located at the upper ring (D110) and near the middle ring (S127) of the extracellular vestibule are directly involved in the evolutionary process that rendered the mammalian α9α10 receptor highly calcium permeable. The introduction of a negative charge at position 110 in α9 mammalian subunits may have enhanced the attraction of calcium ions into the channel vestibule. The change from phenylalanine to serine at position 127 in the mammalian α9 subunits replaced a bulky hydrophobic residue with a small hydrophilic one. This occurred at a strategic location between two major sites for calcium interaction. This amino acid change could have produced a better exposure of the adjacent E129 and D124/D125 to calcium ions and/or may have favored calcium permeability by eliminating the steric hindrance caused by the phenylalanine side chain. The observation that wild-type rat α9α10 nAChRs had a subtle more negative electrostatic potential at the level of S127 than the double D110N/S127F mutant

receptor might support the former. Most important, the results from the analysis of the electrostatic potentials show that the mammalian-specific nonsynonymous substitutions have a long range effect at the deepest region of the vestibule, making the potential significantly less negative, likely favoring the passage of bulky hydrated calcium ions into the transmembrane domain. Contrary to expectation, in the case of chicken receptors the introduction of mammalian-specific residues at positions 110 and 127 produced a long range alteration to a more negative electrostatic potential at the end of the vestibule, likely further impeding the passage of calcium ions into the channel pore and thus accounting for the observation that the introduction of rat residues into a chicken protein background does not increase calcium permeability. Altogether, our functional and in silico study of the vestibule region of α9α10 receptors indicates that the extracellular vestibule participates in divalent to monovalent cation selection and further supports the notion that this region of the channel is involved in the concentration and selection of permeating ions based on electrostatic interactions (Dani 1986; Song and Corry 2009).

A Mammalian-Specific Increase in Calcium Permeability of α9α10 nAChRs

The observation that the introduction of mammalian-specific substitutions within the context of the chicken α9α10 receptor did not completely reproduce the increase in calcium permeability described for mammalian receptors suggests that the consequences of a given substitution greatly depend on the overall sequence (and hence structure) of the protein, a phenomena referred to as epistasis. It is also in agreement with the long standing notion that proteins evolve by a combination of neutral drift and functionally selected substitutions, implying that the effect of an adaptive mutation depends on the presence of other, possibly nonadaptive changes (Zuckerkandl and Pauling 1965; Bloom and Arnold 2009). This has been reported for the evolution of several protein families, including steroid receptors (Bridgham et al. 2009), opsins (Yokoyama et al. 2008), and coral GFP-like proteins (Field and Matz 2010) (reviewed in Harms and Thornton 2010) and extensively documented in directed evolution experiments (Weinreich et al. 2006). It can also be observed while performing horizontal comparisons within the superfamily of Cys-loop receptors, for which nonreciprocal functional effects upon reciprocal amino acid changes have been reported, albeit not fully acknowledged as epistatic in nature (e.g., cation vs. anion selectivity [reviewed in Keramidas et al. 2004] and divalent cation selectivity [Bertrand et al. 1993; Corringer et al. 1999; Fucile et al. 2000; Haghighi and Cooper 2000; Plazas et al. 2005; and this work]). Similar effects have also been demonstrated for horizontal comparisons of calcium permeability on glutamate receptors (Jatzke et al. 2003). The observation that the reciprocal rat/chicken mutations at positions 110 and 127 of the extracellular vestibule of the α9 subunit did not reverse the calcium permeability phenotype, nor produce reciprocal long range changes in electrostatic potentials, indicates the occurrence of

differential epistatic phenomena even between closely related orthologous proteins. In addition, the present results further support the notion that horizontal comparisons rarely identify the combination of residues sufficient to swap the function of one protein to that of another, as they ignore evolutionary history. Horizontal comparisons of extant proteins involve only the ends of the evolutionary tree, whereas protein function evolved as mutations accumulated vertically through time in ancestral protein lineages (Harms and Thornton 2010).

The results presented in this work suggest that the evolutionary processes that brought about the increase on the extent of calcium permeability of $\alpha9\alpha10$ receptors were specific to the mammalian lineage. This receptor participates in the efferent control of cochlear amplification in all vertebrates, thereby modifying the dynamic range of hearing. ACh-mediated receptor opening leads to hyperpolarization of hair cells, which is brought about by activation of calcium sensitive potassium channels (Fuchs and Murrow 1992a, 1992b; Glowatzki and Fuchs 2000). Thus, calcium entry through the $\alpha9\alpha10$ nAChR plays a key role. The selection pressure might have derived from the fact that large conductance, calcium and voltage-gated (BK) potassium channels activated by ACh are expressed at efferent contacts and are the basis for ACh-mediated hyperpolarization of outer hair cells in higher frequency regions of the rat cochlea (Wersinger et al. 2010), compared with cochlear low-frequency regions or the chicken hearing organ, where hair cell hyperpolarization is served by SK potassium channels (Fuchs and Murrow 1992a, 1992b; Glowatzki and Fuchs 2000; Samaranayake et al. 2004). The calcium affinity of BK channels is 2 orders of magnitude lower than that of SK channels (Fakler and Adelman 2008), requiring higher calcium influx for activation. Thus, we propose that three amino acid changes within the $\alpha9$ subunit, together with other lineage-specific background changes, were fixed along mammalian evolutionary history, and rendered the mammalian hair cell nicotinic receptor highly calcium permeable, presumably for enhanced efferent control of the cochlea at high frequencies. These changes most likely complemented other adaptations that support high frequency hearing in mammals, such as the appearance of somatic electromotility in outer hair cells as a means of signal amplification (Manley et al. 2004).

Materials and Methods

All experimental protocols were carried out in accordance with the National Institutes of Health guide for the care and use of laboratory animals as well as Institutional Animal Care and Use Committee of Instituto de Investigaciones en Ingeniería Genética y Biología Molecular.

Expression of Recombinant Receptors in Xenopus laevis Oocytes and Two-Electrode Voltage Clamp

Rat and chicken $\alpha9$ and $\alpha10$ cDNAs constructed in pSGEM, a modified pGEM-HE vector suitable for Xenopus laevis oocyte expression studies, were used as described previously (Elgoyhen et al. 2001; Lipovsek et al. 2012). Capped cRNA

was transcribed in vitro using the RiboMAX Large-Scale RNA Production System (Promega, Madison, WI), with plasmid linearized with NheI. All amino acid substitutions were incorporated by site-directed mutagenesis using the QuickChange II Site-Directed Mutagenesis Kit (Stratagene, La Jolla, CA). Chimeric subunits were generated by means of fusion polymerase chain reaction (PCR) (Szewczyk et al. 2006). Final products were sequenced.

Xenopus laevis frogs were obtained from Nasco (Fort Atkinson, WI). The maintenance of stage V and VI oocytes has been described in detail elsewhere (Katz et al. 2000; Weisstaub et al. 2002). Typically, oocytes were injected with 50 nl of RNase-free water containing 0.01–1.0 ng of cRNAs (at a 1:1 molar ratio) and maintained in Barth's solution at 18 °C.

Electrophysiological recordings were performed 2–6 days after cRNA injection under two-electrode voltage-clamp with a Geneclamp 500 amplifier (Molecular Devices Inc., Sunny Vale, CA). Both voltage and current electrodes were filled with 3 M KCl and had resistances of approximately 1–2 MΩ. The preparation was grounded by means of an Ag/AgCl wire in a 3 M KCl solution connected to the bath through a 3 M KCl agar bridge. During electrophysiological recordings, oocytes were continuously superfused (~10 ml/min) with normal frog saline comprised of (mM): 115 NaCl, 2.5 KCl, 1.8 CaCl$_2$, and 10 HEPES buffer, pH 7.2. ACh was applied in the perfusion solution of the oocyte chamber.

In order to minimize the activation of the native oocyte's Ca^{2+}-sensitive chloride current, ICl_{Ca} (Barish 1983), by Ca^{2+} entering through nAChRs, all experiments, unless otherwise stated, were carried out in oocytes incubated with the membrane permeant Ca^{2+} chelator BAPTA-AM (100 μM) for 3 h prior to electrophysiological recordings. This treatment has been previously shown to effectively chelate intracellular Ca^{2+} ions and, therefore, to impair the activation of the ICl_{Ca} (Katz et al. 2000). In order to minimize the activation of the oocyte's nonselective inward current through a hemigap junction channel in response to the reduction of the external divalent cation concentration, all experiments were carried out in oocytes injected with 7.5 ng of an oligonucleotide (5′-GCTTTAG TAATTCCCATCCTGCCATGTTTC-3′) antisense to connexin C38 mRNA (Ebihara 1996).

In order to assess whether calcium ions are a major component of the inward nicotinic current on the different $\alpha9/\alpha10$ receptors, we took advantage of the oocyte's endogenous Ca^{2+}-dependent Cl^{-} channels as indirect reporters of calcium entry through activated $\alpha9$ and/or $\alpha10$ nAChRs. Current amplitudes were measured, on normal frog saline, on the same oocyte before and after a 3-h incubation in BAPTA-AM. The percentage of the initial response remaining after BAPTA incubation was determined for each oocyte individually. Mean ± SEM of the percentage response after BAPTA was then determined for each receptor.

The solution used for monovalent cation permeability studies (pK/pNa) was, in mM: 10 HEPES, 0.5 CaCl$_2$, 2 KCl, 10–96 NaCl, and 20–110 N-methyl glucamine (NMG$^+$) in order to compensate for changes in osmolarity, pH adjusted

to 7.2 with HCl. The solution used for the calcium permeability studies (pCa/pNa) was, in mM: 10 HEPES, 0.2–5 $CaCl_2$, and 100–120 NMG^+ in order to compensate for changes in osmolarity, pH adjusted to 7.2 with HCl. In all the experiments, oocytes were superfused for 2 min with the test solution before the application of ACh and were transferred back to normal frog saline for at least 3 min before changing to a different test solution.

I–V relationships were obtained by applying 2-s voltage ramps from −120 to +50 mV, at the plateau response to 10 or 100 μM ACh from a holding potential (V_{hold}) of −70 mV. Leakage correction was performed by digital subtraction of the I–V curve obtained by the same voltage ramp protocol prior to the application of ACh. Generation of voltage protocols and data acquisition was performed using a Digidata 1200 and the pClamp 7.0 software (Molecular Devices Inc.). Data were analyzed using Clamp Fit from the pClamp7.0 software and Graph Pad Prism 6.00 for Windows (GraphPad Software, San Diego, CA).

The relative Ca^{2+} to monovalent permeability was evaluated by analyzing the shift in the reversal potential (E_{rev}) as a function of the extracellular Ca^{2+} concentration. All monovalent cations in the extracellular medium were replaced by the impermeant monovalent cation NMG^+ in order to enhance the shift in E_{rev} upon variation of Ca^{2+}, as previously described (Ferrer-Montiel and Montal 1993; Katz et al. 2000; Sgard et al. 2002; Weisstaub et al. 2002). The internal concentrations of Na^+ and K^+ used in the calculations were 10 and 110 mM, respectively (Costa et al. 1989). The relative pCa/pNa was calculated with the GHK constant field voltage equation assuming no anion permeability and extended to include divalent cations (Lewis 1979). The relative pK/pNa used for the calculations was experimentally determined for all receptors by analyzing the shift in the reversal potential (E_{rev}) as a function of the extracellular Na^+ concentration and fitting the data to the GHK equation as previously described (Bertrand et al. 1993; Ferrer-Montiel and Montal 1993). Permeability ratios were calculated for each oocyte and then averaged; values are the mean ± SEM. E_{rev} in normal frog saline was determined for all receptors to further evaluate monovalent relative permeability. The pK/pNa values obtained are depicted in supplementary table S4, Supplementary Material online.

For several mutant receptors evaluated we identified a change in the pK/pNa relative monovalent cation permeability, with respect to that of the corresponding wild-type receptor. For these mutant receptors, we also observed a significant change in the E_{rev} determined in normal frog saline (supplementary table S4, Supplementary Material online). As $\alpha9\alpha10$ receptors show a very prominent K^+ outward current that contributes to the E_{rev}, these changes in pK/pNa had a profound effect on the E_{rev} shifts observed while changing the extracellular calcium concentration. In those cases, in order to compare the shifts in E_{rev} elicited by changes in extracellular calcium concentration independently of the differences in pK/pNa between mutant and wild-type receptors, the E_{rev} values of the mutant receptors, plotted in the E_{rev} versus $[Ca^{2+}]$ graphs were normalized to the values as expected for the pK/pNa determined for the corresponding wild-type receptor.

Statistics and Reagents

Statistical analysis was performed on Graph Pad Prism 6.00 for Windows (GraphPad Software). Statistical significance was evaluated by the Student's t-test (two-tailed, unpaired samples), corrected for multiple comparisons using the Holm–Sidak method. $P < 0.05$ was considered significant. All salts, BAPTA-AM, NMG^+, HEPES, and ACh chloride were purchased from Sigma Chemical Co. ACh chloride was dissolved in distilled water as a 100 mM stock and stored in aliquots at −20 °C. BAPTA-AM was stored at −20 °C as aliquots of a 100 mM solution in dimethyl sulfoxide, thawed, and diluted 1,000-fold into Barth's solution shortly before incubation of the oocytes.

Sequence Analysis and Ancestral Sequence Reconstruction

Coding sequences for the $\alpha9$ subunit of 52 vertebrate species were downloaded from GenBank (www.ncbi.nlm.nih.gov/genbank, last accessed September 11, 2014), Ensembl (www.ensembl.org, last accessed September 11, 2014), or UCSC (http://genome.ucsc.edu/, last accessed September 11, 2014) databases. The alignment used for the branch-site test for positive selection and ancestral sequence reconstruction is shown in supplementary figure S1, Supplementary Material online, and accession numbers are listed in supplementary table S2, Supplementary Material online. All sequences were visually inspected, and missing exons were obtained from the NCBI Genome Project traces database (http://blast.ncbi.nlm.nih.gov/Blast.cgi, last accessed September 11, 2014). Sequence alignment was performed using the ClustalW tool implemented in the MEGA5 software (Tamura et al. 2011) (www.megasoftware.net, last accessed September 11, 2014), visually inspected, and manually edited.

To test for the presence of positive selection, we applied the branch-site test of positive selection developed by Yang and coworkers (Yang 2007; Yang and Nielsen 2002; Zhang et al. 2005) using the "codeml" program implemented in PAML. The branch-site model allows ω, the ratio of nonsynonymous to synonymous substitution rate, to vary both among sites in the protein and across branches on the tree and requires the a priori specification of foreground (the branch of interest) and background (all other branches) lineages within the phylogeny. Accordingly, the analysis assigns each site in the protein to one of three site classes. Class 0 and 1 sites include codons that are conserved ($0 < \omega_0 < 1$) or neutral ($\omega_1 = 1$) throughout the tree and have the same ω value in the background and foreground lineages; codons assigned to class 2 sites are conserved or neutral on the background branches but become under positive selection on the foreground branches, with $\omega_2 > 1$. The test aims to detect positive selection affecting a few sites along the foreground lineage (the class 2 sites) by comparing the branch-site model (H_A), in which class 2 sites are under positive selection (with $\omega_2 > 1$), to a null model (H_0) in which class 2 sites are neutral

(with $\omega_1 = 1$) through a likelihood ratio test (LRT). The LRT (twice the log-likelihood difference between the two models) is compared with a χ^2 distribution with the degrees of freedom equal to the difference in parameters between the two models. This analysis was conducted separately three times, using either the mammalian, eutherian, or saur-opsid lineages as foreground lineages.

With the exception of the C-terminal portion which is conserved and forms a well-described α-helix (the MA α-helix), the intracellular domain located between TM3 and TM4 is the most variable region of all nicotinic subunits show-ing a great number of insertions, deletions, and nonsynony-mous substitutions, even when comparing the same subunit from different species. This precludes the accurate prediction of ancestral sequences for this portion of the protein and was therefore not included it in the ancestral sequence recon-struction analysis.

Ancestral sequence reconstruction was performed on the Datamonkey web server (http://www.datamonkey.org/, last accessed September 11, 2014) (Delport et al. 2010), imple-menting a model-based, maximum-likelihood approach (Yang et al. 1995). For the nucleotide sequences, the best-fitting nucleotide model was inferred from the alignment. For amino acid sequences, the JTT rate matrix (Jones et al. 1992) was determined to best fit the data and used in the analysis. The character state and its marginal posterior probability were determined for each site at each of the internal nodes of the phylogeny depicted in supplementary figure S2, Supplementary Material online. Inferred sequences for the major nodes are included in the alignment of supplementary figure S1, Supplementary Material online.

Homology Modeling, MD Simulation, and Determination of Electrostatic Potentials

We used the comparative protein structural modeling pro-gram, MODELLER9v6 (Sali and Blundell 1993) to generate homology models of the rat and chicken $\alpha9\alpha10$ nAChRs, wild type and 110 and 127 mutants, using the *Torpedo* nAChR structural model (2BG9; Unwin 2005) as template. Alignment was performed using the Multalin server (Corpet 1988). Modeling was performed using standard pa-rameters, for 100 runs. The outcomes were ranked on the basis of the internal scoring function and the best models were chosen.

For the MD simulations performed on the wild-type $\alpha9\alpha10$ nAChR, the best model chosen from the homology modelling was used as the target model and imbedded in a fully solvated 1-palmitoyl-2-oleoyl-sn-glycero-3-phos-phocholine lipid bilayer, using water model TIP3 to solvate. Ions were added creating an overall neutral system in approx-imately 0.13 M NaCl using the VMD software (Humphrey et al. 1996). The ions were equally distributed in a water box. The final system contained approximately 400,000 atoms and was submitted to MD simulation for 1 ns using NAMD 2.6 (Phillips et al. 2005). The NPT ensemble was used to perform MD calculations. Periodic boundary conditions were applied to the system in the three coordinate directions.

A pressure of 1 atm and a temperature of 310 K were main-tained throughout.

To represent the receptor structure in an active state a molecular docking of ACh was performed, using AutoDock 4.0 suite, on every binding site (Morris et al. 1998). The grid maps were calculated using the autogrid4 option and were centered on the ligand-binding sites. The volumes chosen for the grid maps were made up of $60 \times 60 \times 60$ points, with a grid-point spacing of 0.375 Å. The autotors option was used to define the rotating bond in the ligand. In the Lamarckian genetic algorithm dockings, an initial population of random individuals of 1,500 with a population size of 50 individuals, a maximum number of 2.5×10^6 energy evaluations, a maxi-mum number generations of 27,000, a mutation rate of 0.02, and cross-over rate of 0.80 were employed. The docked com-pound complexes were built using the lowest docked-energy binding positions. ACh was constructed using Gaussian03 (Frisch et al. 2004) and the partial charges of different com-pounds were corrected using ESP methodology.

For the MD simulation of Ca^{2+} permeation, the cation was initially centered on the upper end of the channel. Using constant velocity SMD simulations on an equilibrated recep-tor/Ca^{2+} complex and the corresponding ligand on the re-ceptor's binding sites, main interactions were evaluated. Ca^{2+} coordinates were determinate using an average of distances between subunits. Force was applied on the calcium ion through a connecting spring adhered at its center of mass, with a velocity of 0.00001 Å/time step and a harmonic con-stant of 6 kcal/(mol Å^2). The NAMD program and Charmm27 force field were used at 310 K, 1 atm and simulation time was 1.25 ns. Figures were generated using the PyMOL Molecular Graphics System (Version 1.5.0.4 Schrödinger, LLC).

The electrostatic potential of the rat and chicken $\alpha9\alpha10$ receptors, wild type and mutant, was determined using Adaptive Poisson Boltzmann Solver (Baker et al. 2001). The linearized Poisson–Boltzmann equation was solved for each protein without ligands. Calculation parameters for protein dielectric, solvent dielectric, and temperature were 2.0, 78.5, and 298.15 K, respectively. VMD software (Humphrey et al. 1996) was used to visualize electrostatic potentials on a lon-gitudinal plane that cuts through the middle of the receptors. The electrostatic potential values for the central Z axis were obtained from the DX files using the potential.py script (Baker et al. 2001).

Supplementary Material

Supplementary figures S1–S4 and tables S1–S4 are available at *Molecular Biology and Evolution* online (http://www.mbe.oxfordjournals.org/).

Acknowledgments

References

Baker NA, Sept D, Joseph S, Holst MJ, McCammon JA. 2001. Electrostatics of nanosystems: application to microtubules and the ribosome. *Proc Natl Acad Sci U S A.* 98:10037–10041.

Barish ME. 1983. A transient calcium-dependent chloride current in the immature *Xenopus* oocyte. *J Physiol.* 342:309–325.

Bertrand D, Galzi JL, Devillers-Thiery A, Bertrand S, Changeux JP. 1993. Mutations at two distinct sites within the channel domain M2 alter calcium permeability of neuronal alpha 7 nicotinic receptor. *Proc Natl Acad Sci U S A.* 90:6971–6975.

Bloom JD, Arnold FH. 2009. In the light of directed evolution: pathways of adaptive protein evolution. *Proc Natl Acad Sci U S A.* 106 (Suppl 1), 9995–10000.

Bridgham JT, Ortlund EA, Thornton JW. 2009. An epistatic ratchet constrains the direction of glucocorticoid receptor evolution. *Nature* 461:515–519.

Cohen BN, Labarca C, Davidson N, Lester HA. 1992. Mutations in M2 alter the selectivity of the mouse nicotinic acetylcholine receptor for organic and alkali metal cations. *J Gen Physiol.* 100:373–400.

Colon-Saez JO, Yakel JL. 2014. A mutation in the extracellular domain of the alpha7 nAChR reduces calcium permeability. *Pflugers Arch.* 466(8):1571–1579.

Corpet F. 1988. Multiple sequence alignment with hierarchical clustering. *Nucleic Acids Res.* 16:10881–10890.

Corringer PJ, Bertrand S, Galzi JL, Devillers-Thiery A, Changeux JP, Bertrand D. 1999. Mutational analysis of the charge selectivity filter of the alpha7 nicotinic acetylcholine receptor. *Neuron* 22: 831–843.

Corringer PJ, Le Novere N, Changeux JP. 2000. Nicotinic receptors at the amino acid level. *Annu Rev Pharmacol Toxicol.* 40:431–458.

Costa PF, Emilio MG, Fernandes PL, Ferreira HG, Ferreira KG. 1989. Determination of ionic permeability coefficients of the plasma membrane of *Xenopus laevis* oocytes under voltage clamp. *J Physiol.* 413:199–211.

Dallos P, Wu X, Cheatham MA, Gao J, Zheng J, Anderson CT, Jia S, Wang X, Cheng WH, Sengupta S, et al. 2008. Prestin-based outer hair cell motility is necessary for mammalian cochlear amplification. *Neuron* 58:333–339.

Dani JA. 1986. Ion-channel entrances influence permeation. Net charge, size, shape, and binding considerations. *Biophys J.* 49:607–618.

Dani JA, Bertrand D. 2007. Nicotinic acetylcholine receptors and nicotinic cholinergic mechanisms of the central nervous system. *Annu Rev Pharmacol Toxicol.* 47:699–729.

Delport W, Poon AF, Frost SD, Kosakovsky Pond SL. 2010. Datamonkey 2010: a suite of phylogenetic analysis tools for evolutionary biology. *Bioinformatics* 26:2455–2457.

Dent JA. 2006. Evidence for a diverse Cys-loop ligand-gated ion channel superfamily in early bilateria. *J Mol Evol.* 62:523–535.

Di Castro A, Martinello K, Grassi F, Eusebi F, Engel AG. 2007. Pathogenic point mutations in a transmembrane domain of the epsilon subunit increase the Ca2+ permeability of the human endplate ACh receptor. *J Physiol.* 579:671–677.

Ebihara L. 1996. *Xenopus* connexin38 forms hemi-gap-junctional channels in the nonjunctional plasma membrane of *Xenopus* oocytes. *Biophys J.* 71:742–748.

Elgoyhen AB, Katz E. 2012. The efferent medial olivocochlear-hair cell synapse. *J Physiol Paris.* 106:47–56.

Elgoyhen AB, Vetter DE, Katz E, Rothlin CV, Heinemann SF, Boulter J. 2001. alpha10: a determinant of nicotinic cholinergic receptor function in mammalian vestibular and cochlear mechanosensory hair cells. *Proc Natl Acad Sci U S A.* 98:3501–3506.

Fakler B, Adelman JP. 2008. Control of K(Ca) channels by calcium nano/microdomains. *Neuron* 59:873–881.

Ferrer-Montiel AV, Montal M. 1993. A negative charge in the M2 transmembrane segment of the neuronal alpha 7 acetylcholine receptor increases permeability to divalent cations. *FEBS Lett.* 324: 185–190.

Field SF, Matz MV. 2010. Retracing evolution of red fluorescence in GFP-like proteins from Faviina corals. *Mol Biol Evol.* 27:225–233.

Franchini LF, Elgoyhen AB. 2006. Adaptive evolution in mammalian proteins involved in cochlear outer hair cell electromotility. *Mol Phylogenet Evol.* 41:622–635.

Frisch MJ, Trucks GW, Schlegel HB, Scuseria GE, Robb MA, Cheeseman JR, Montgomery JA Jr, Vreven T, Kudin KN, Burant JC, et al. 2004. Gaussian 03, Revision C.02. Wallingford (CT): Gaussian, Inc.

Fuchs PA, Murrow BW. 1992a. Cholinergic inhibition of short (outer) hair cells of the chick's cochlea. *J Neurosci.* 12:800–809.

Fuchs PA, Murrow BW. 1992b. A novel cholinergic receptor mediates inhibition of chick cochlear hair cells. *Proc Biol Sci.* 248:35–40.

Fucile S, Palma E, Mileo AM, Miledi R, Eusebi F. 2000. Human neuronal threonine-for-leucine-248 alpha 7 mutant nicotinic acetylcholine receptors are highly Ca2+ permeable. *Proc Natl Acad Sci U S A.* 97:3643–3648.

Fucile S, Sucapane A, Eusebi F. 2006. Ca2+ permeability through rat cloned alpha9-containing nicotinic acetylcholine receptors. *Cell Calcium* 39:349–355.

Fucile S, Sucapane A, Grassi F, Eusebi F, Engel AG. 2006. The human adult subtype ACh receptor channel has high Ca2+ permeability and predisposes to endplate Ca2+ overloading. *J Physiol.* 573:35–43.

Galzi JL, Devillers-Thiery A, Hussy N, Bertrand S, Changeux JP, Bertrand D. 1992. Mutations in the channel domain of a neuronal nicotinic receptor convert ion selectivity from cationic to anionic. *Nature* 359: 500–505.

Gay EA, Yakel JL. 2007. Gating of nicotinic ACh receptors; new insights into structural transitions triggered by agonist binding that induce channel opening. *J Physiol.* 584:727–733.

Giniatullin R, Nistri A, Yakel JL. 2005. Desensitization of nicotinic ACh receptors: shaping cholinergic signaling. *Trends Neurosci.* 28: 371–378.

Glowatzki E, Fuchs PA. 2000. Cholinergic synaptic inhibition of inner hair cells in the neonatal mammalian cochlea. *Science* 288: 2366–2368.

Haghighi AP, Cooper E. 2000. A molecular link between inward rectification and calcium permeability of neuronal nicotinic acetylcholine alpha3beta4 and alpha4beta2 receptors. *J Neurosci.* 20:529–541.

Hansen SB, Wang HL, Taylor P, Sine SM. 2008. An ion selectivity filter in the extracellular domain of Cys-loop receptors reveals determinants for ion conductance. *J Biol Chem.* 283:36066–36070.

Harms MJ, Thornton JW. 2010. Analyzing protein structure and function using ancestral gene reconstruction. *Curr Opin Struct Biol.* 20: 360–366.

Hughes AL. 2008. The origin of adaptive phenotypes. *Proc Natl Acad Sci U S A.* 105:13193–13194.

Humphrey W, Dalke A, Schulten K. 1996. VMD: visual molecular dynamics. *J Mol Graph.* 14:33–38, 27–38.

Imoto K, Busch C, Sakmann B, Mishina M, Konno T, Nakai J, Bujo H, Mori Y, Fukuda K, Numa S. 1988. Rings of negatively charged amino acids determine the acetylcholine receptor channel conductance. *Nature* 335:645–648.

Imoto K, Konno T, Nakai J, Wang F, Mishina M, Numa S. 1991. A ring of uncharged polar amino acids as a component of channel constriction in the nicotinic acetylcholine receptor. *FEBS Lett.* 289: 193–200.

Jatzke C, Hernandez M, Wollmuth LP. 2003. Extracellular vestibule determinants of Ca2+ influx in Ca2+-permeable AMPA receptor channels. *J Physiol.* 549:439–452.

Jensen ML, Schousboe A, Ahring PK. 2005. Charge selectivity of the Cys-loop family of ligand-gated ion channels. *J Neurochem.* 92: 217–225.

Jones DT, Taylor WR, Thornton JM. 1992. The rapid generation of mutation data matrices from protein sequences. *Comput Appl Biosci.* 8: 275–282.

Karlin A. 2002. Emerging structure of the nicotinic acetylcholine receptors. Nat Rev Neurosci. 3:102–114.

Katz E, Verbitsky M, Rothlin CV, Vetter DE, Heinemann SF, Elgoyhen AB. 2000. High calcium permeability and calcium block of the alpha9 nicotinic acetylcholine receptor. Hear Res. 141:117–128.

Kaupp UB, Seifert R. 2002. Cyclic nucleotide-gated ion channels. Physiol Rev. 82:769–824.

Keramidas A, Moorhouse AJ, Schofield PR, Barry PH. 2004. Ligand-gated ion channels: mechanisms underlying ion selectivity. Prog Biophys Mol Biol. 86:161–204.

Konno T, Busch C, Von Kitzing E, Imoto K, Wang F, Nakai J, Mishina M, Numa S, Sakmann B. 1991. Rings of anionic amino acids as structural determinants of ion selectivity in the acetylcholine receptor channel. Proc Biol Sci. 244:69–79.

Laude AJ, Simpson AW. 2009. Compartmentalized signalling: Ca2+ compartments, microdomains and the many facets of Ca2+ signalling. FEBS J. 276:1800–1816.

Leonard RJ, Labarca CG, Charnet P, Davidson N, Lester HA. 1988. Evidence that the M2 membrane-spanning region lines the ion channel pore of the nicotinic receptor. Science 242:1578–1581.

Lewis CA. 1979. Ion-concentration dependence of the reversal potential and the single channel conductance of ion channels at the frog neuromuscular junction. J Physiol. 286:417–445.

Lipovsek M, Im GJ, Franchini LF, Pisciottano F, Katz E, Fuchs PA, Elgoyhen AB. 2012. Phylogenetic differences in calcium permeability of the auditory hair cell cholinergic nicotinic receptor. Proc Natl Acad Sci U S A. 109:4308–4313.

Livesey MR, Cooper MA, Lambert JJ, Peters JA. 2011. Rings of charge within the extracellular vestibule influence ion permeation of the 5-HT3A receptor. J Biol Chem. 286:16008–16017.

Manley GA, Popper AN, Fay RR. 2004. Evolution of the vertebrate auditory system. New York: Springer-Verlag.

Mayer ML, Westbrook GL. 1987. Permeation and block of N-methyl-D-aspartic acid receptor channels by divalent cations in mouse cultured central neurones. J Physiol. 394:501–527.

Miledi R, Parker I, Woodward RM. 1989. Membrane currents elicited by divalent cations in Xenopus oocytes. J Physiol. 417:173–195.

Miller C. 1989. Genetic manipulation of ion channels: a new approach to structure and mechanism. Neuron 2:1195–1205.

Morris GM, Goodsell DS, Halliday RS, Huey R, Hart WE, Belew RK, Olson AJ. 1998. Automated docking using a lamarckian genetic algorithm and an empirical binding free energy function. J Comput Chem. 19: 1639–1662.

Peters JA, Cooper MA, Carland JE, Livesey MR, Hales TG, Lambert JJ. 2010. Novel structural determinants of single channel conductance and ion selectivity in 5-hydroxytryptamine type 3 and nicotinic acetylcholine receptors. J Physiol. 588:587–596.

Phillips JC, Braun R, Wang W, Gumbart J, Tajkhorshid E, Villa E, Chipot C, Skeel RD, Kale L, Schulten K. 2005. Scalable molecular dynamics with NAMD. J Comput Chem. 26:1781–1802.

Plazas PV, De Rosa MJ, Gomez-Casati ME, Verbitsky M, Weisstaub N, Katz E, Bouzat C, Elgoyhen AB. 2005. Key roles of hydrophobic rings of TM2 in gating of the alpha9alpha10 nicotinic cholinergic receptor. Br J Pharmacol. 145:963–974.

Sali A, Blundell TL. 1993. Comparative protein modelling by satisfaction of spatial restraints. J Mol Biol. 234:779–815.

Samaranayake H, Saunders JC, Greene MI, Navaratnam DS. 2004. Ca(2+) and K(+) (BK) channels in chick hair cells are clustered and colocalized with apical-basal and tonotopic gradients. J Physiol. 560: 13–20.

Seguela P, Wadiche J, Dineley-Miller K, Dani JA, Patrick JW. 1993. Molecular cloning, functional properties, and distribution of rat brain alpha 7: a nicotinic cation channel highly permeable to calcium. J Neurosci. 13:596–604.

Sgard F, Charpantier E, Bertrand S, Walker N, Caput D, Graham D, Bertrand D, Besnard F. 2002. A novel human nicotinic receptor subunit, alpha10, that confers functionality to the alpha9-subunit. Mol Pharmacol. 61:150–159.

Shen JX, Yakel JL. 2009. Nicotinic acetylcholine receptor-mediated calcium signaling in the nervous system. Acta Pharmacol Sin. 30: 673–680.

Song C, Corry B. 2009. Role of acetylcholine receptor domains in ion selectivity. Biochim Biophys Acta. 1788:1466–1473.

Sutton KA, Jungnickel MK, Jovine L, Florman HM. 2012. Evolution of the voltage sensor domain of the voltage-sensitive phosphoinositide phosphatase VSP/TPTE suggests a role as a proton channel in eutherian mammals. Mol Biol Evol. 29:2147–2155.

Szewczyk E, Nayak T, Oakley CE, Edgerton H, Xiong Y, Taheri-Talesh N, Osmani SA, Oakley BR. 2006. Fusion PCR and gene targeting in Aspergillus nidulans. Nat Protoc. 1:3111–3120.

Tamura K, Peterson D, Peterson N, Stecher G, Nei M, Kumar S. 2011. MEGA5: molecular evolutionary genetics analysis using maximum likelihood, evolutionary distance, and maximum parsimony methods. Mol Biol Evol. 28:2731–2739.

Tapia L, Kuryatov A, Lindstrom J. 2007. Ca2+ permeability of the (alpha4)3(beta2)2 stoichiometry greatly exceeds that of (alpha4)2(-beta2)3 human acetylcholine receptors. Mol Pharmacol. 71:769–776.

Unwin N. 2005. Refined structure of the nicotinic acetylcholine receptor at 4A resolution. J Mol Biol. 346:967–989.

Villarroel A, Herlitze S, Koenen M, Sakmann B. 1991. Location of a threonine residue in the alpha-subunit M2 transmembrane segment that determines the ion flow through the acetylcholine receptor channel. Proc Biol Sci. 243:69–74.

Villarroel A, Sakmann B. 1992. Threonine in the selectivity filter of the acetylcholine receptor channel. Biophys J. 62:196–205; discussion 205–198.

Wang F, Imoto K. 1992. Pore size and negative charge as structural determinants of permeability in the Torpedo nicotinic acetylcholine receptor channel. Proc Biol Sci. 250:11–17.

Wang HL, Cheng X, Taylor P, McCammon JA, Sine SM. 2008. Control of cation permeation through the nicotinic receptor channel. PLoS Comput Biol. 4:e41.

Weinreich DM, Delaney NF, Depristo MA, Hartl DL. 2006. Darwinian evolution can follow only very few mutational paths to fitter proteins. Science 312:111–114.

Weisstaub N, Vetter DE, Elgoyhen AB, Katz E. 2002. The alpha9alpha10 nicotinic acetylcholine receptor is permeable to and is modulated by divalent cations. Hear Res. 167:122–135.

Wersinger E, McLean WJ, Fuchs PA, Pyott SJ. 2010. BK channels mediate cholinergic inhibition of high frequency cochlear hair cells. PLoS One 5:e13836.

Yang Z. 2007. PAML 4: phylogenetic analysis by maximum likelihood. Mol Biol Evol. 24:1586–1591.

Yang Z, Kumar S, Nei M. 1995. A new method of inference of ancestral nucleotide and amino acid sequences. Genetics 141:1641–1650.

Yang Z, Nielsen R. 2002. Codon-substitution models for detecting molecular adaptation at individual sites along specific lineages. Mol Biol Evol. 19:908–917.

Yokoyama S, Yang H, Starmer WT. 2008. Molecular basis of spectral tuning in the red- and green-sensitive (M/LWS) pigments in vertebrates. Genetics 179:2037–2043.

Zhang J, Nielsen R, Yang Z. 2005. Evaluation of an improved branch-site likelihood method for detecting positive selection at the molecular level. Mol Biol Evol. 22:2472–2479.

Zuckerkandl E, Pauling L. 1965. Evolutionary divergence and convergence in proteins. New York: Springer.